nature portfolio

https://doi.org/10.1038/s41561-022-01017-x

Supplementary information

Carbon and sediment fluxes inhibited in the submarine Congo Canyon by landslide-damming

In the format provided by the authors and unedited

Extended Data Figures

Extended Data Figure 1. Two other possible canyon-flank landslides identified in the 2019 bathymetry. a) Possible landslide headscarp and deposit which are interpreted to have involved similar processes to those envisaged for the canyon-flank landslide seen in Fig. 2. b) Canyon-flank landslide appears to constrict the canyon floor leading to the development of a new thalweg channel due to enhanced turbidity current erosional capacity. Processes envisaged here are similar to those described in Fig. 4a, c.

Supplementary material

SM1. Other possible canyon-flank landslides in the 2019 data

Other features visible in the 2019 bathymetry data are also interpreted as potential canyon-flank landside deposits (SFig. 1). However, in neither case did the canyon-flank landslide occur between 2005 and 2019. Therefore, we cannot say for certain that the interpreted morphology is a consequence of a canyon-flank landslide. A first possible headscarp and deposit, with similar morphologies to that seen in the upper part of the study area (Fig. 2b), are located at 1980 m water depth on the northern canyon-flank (SFig. 1a). If indeed a canyon-flank landslide, the headwall is 200 m high and 290 m wide with a perimeter of 1.73 km. Here, the main canyon thalweg is situated between the landslide headscarp and the interpreted deposit. The shape of the infill is suggestive of a palaeo-meander which has been cut-off.

A second potential landslide complex with a different morphology is observed at 1300 m water depth on the northern canyon-flank, at the eastern end of the study area (SFig. 1b). Here, multiple headscarps are associated with a lobate deposit covering 0.65 km^2. The deposit constricts the canyon thalweg, but does not block it. A channel, which has been incised into the canyon floor meanders around the landslide deposit with a knickpoint up-canyon of the deposit (SFig. 1b). The channel is 6 km long with a maximum depth and width of 10 and 200 m, respectively. We interpret the processes associated with this canyon-flank landslide to be similar to those described in Fig. 4a, c.

Supplementary Tables

Supplementary Table 1. Submarine canyons where high resolution multibeam bathymetry is available. Studies which include repeat multibeam bathymetry similar to this study are identified. Mass wasting features, terraces and canyon sidewalls similar to those observed in this study are described. Bathymetry examples of the described features are also shown. For example, terraces are identified which are likely to be areas of high sediment accumulation, and may be prone to collapse. Other examples where submarine canyons exhibit similar seafloor geomorphic features in 3-D seismic data, such as the Niger Channel, but where bathymetric data has not been published have been omitted.

Canyon/ Margin	Date of Survey	Multibeam bathymetry resolution (m)	Reference	Description of mass wasting or terrace features	Swath bathymetry of submarine canyon showing similar landslide or terrace features as identified in the Congo Canyon
Dohrn	2000 - 2014	10	Aiello et al. 2020[51]	Landslide scars located around the rim of the canyon. Additional slope failure deposits identifiable in seismic profile data	
Magnaghi	2000 - 2014	10	Aiello et al. 2020[51]	Slope failure deposits identifiable in seismic profile data	

Andøya	2004, 2005	5 (shallower than 1000 m) 25 (deeper than 1000 m)	Amundsen et al. 2015[52] Laberg et al. 2007[53]	Landslide headwalls visible in bathymetry.	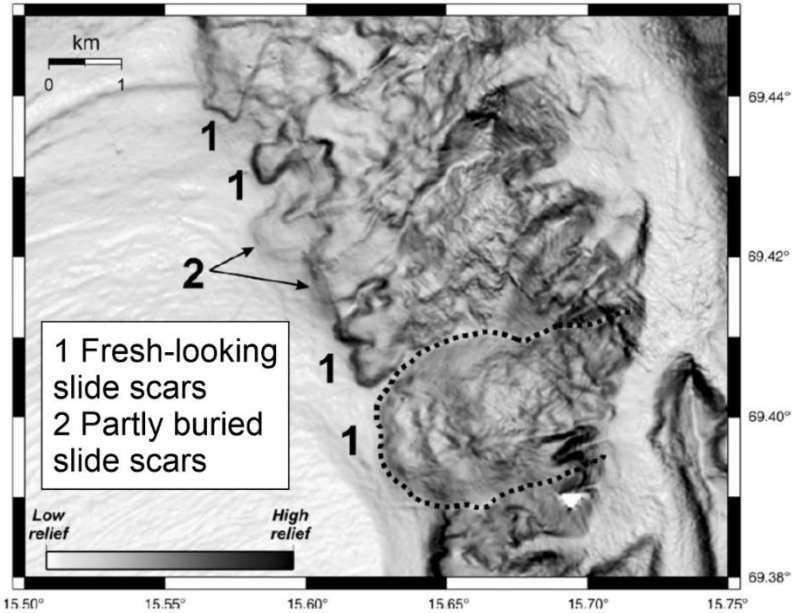
Cap Timiris	2003	Not reported	Antrobreh and Krastel 2006[54]	Slump deposits identifiable in canyon thalweg from steep canyon walls. Similar arcuate terrace features to Congo Canyon	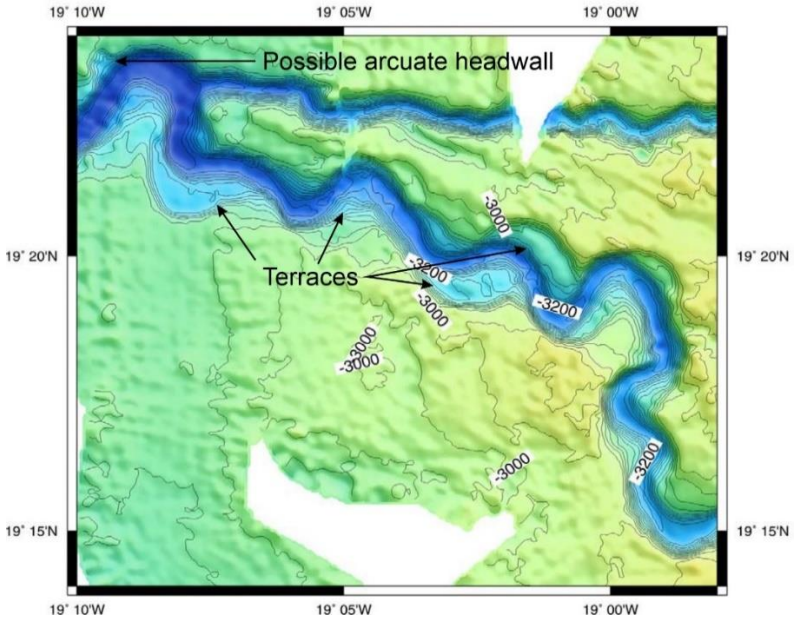

Bourcart	1995 – 2002	Not reported	Baztan et al. 2005[55]	Slide headwalls visible in bathymetry and seismic cross sections	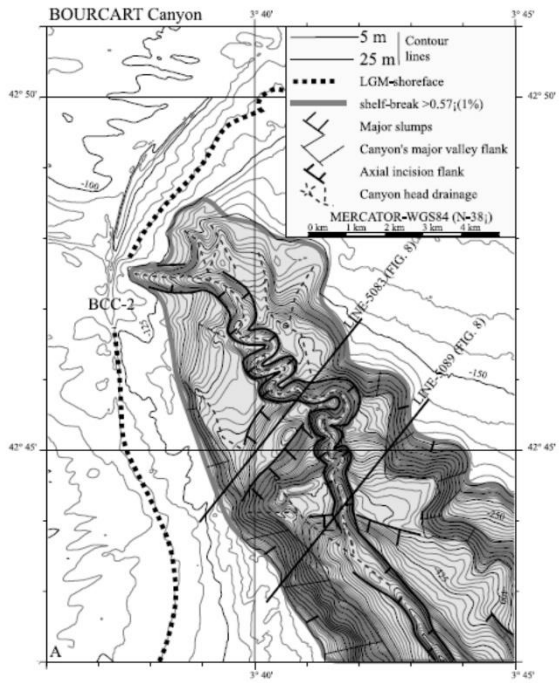
Biobío	2011	5	Bernhardt et al. 2015[56]	Arcuate headscarps present with hummocky material partially blocking the canyon. Additional detachment surfaces are visible in	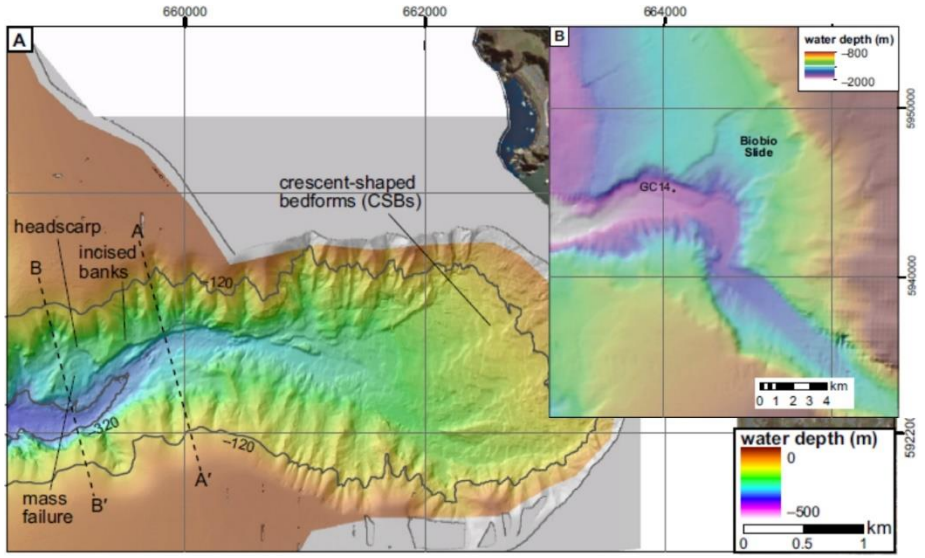

				seismic profiles	
Cap Lopez	2004 – 2008 (repeat bathymetry)	10	Biscara et al. 2013[57]	Canyon flank landslide identified. Estimated mass of 95,000 m^3 ± 15,000 m^3. 60% of thalweg deposit reworked within one year.	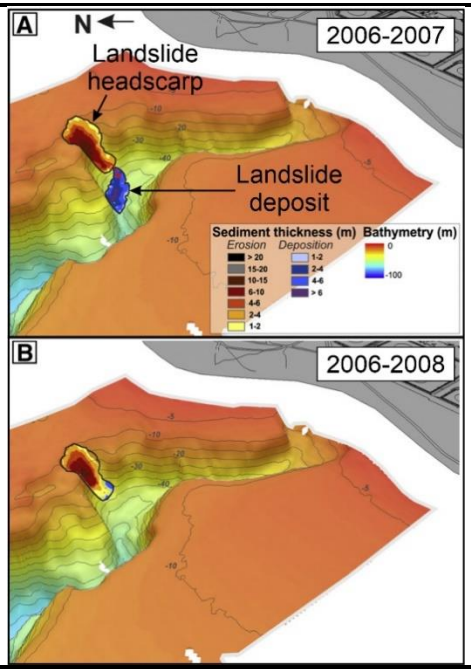

Cape D'Orlando Basin	2011, 2012	1 (0 – 100 m water depth) 20 (100 – 1000 m water depth	Casalbore et al. 2020[58]	280 landslide scars recognised in bathymetry down to 550 m water depth.	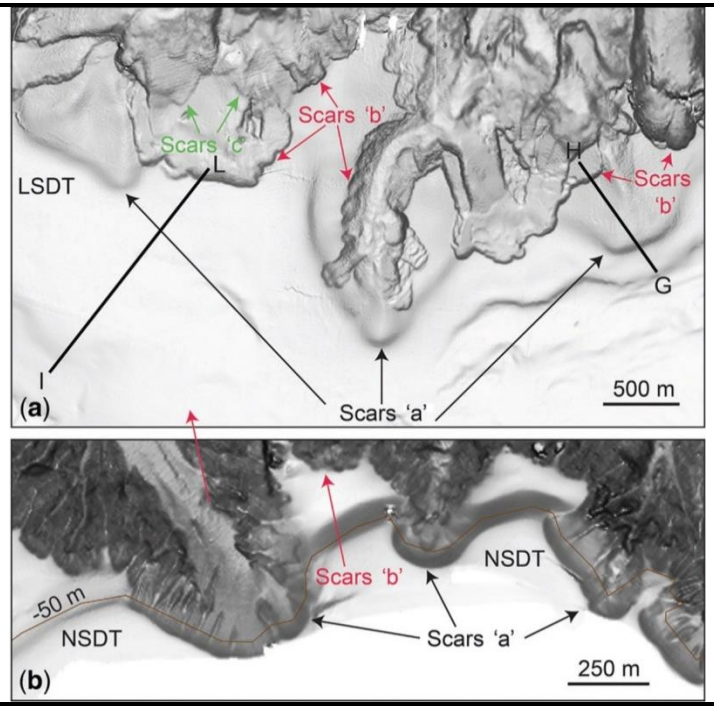
Areia Branca	2011	50	de Almedia et al. 2015[59]	Arcuate headwalls with the presence of marginal terraces	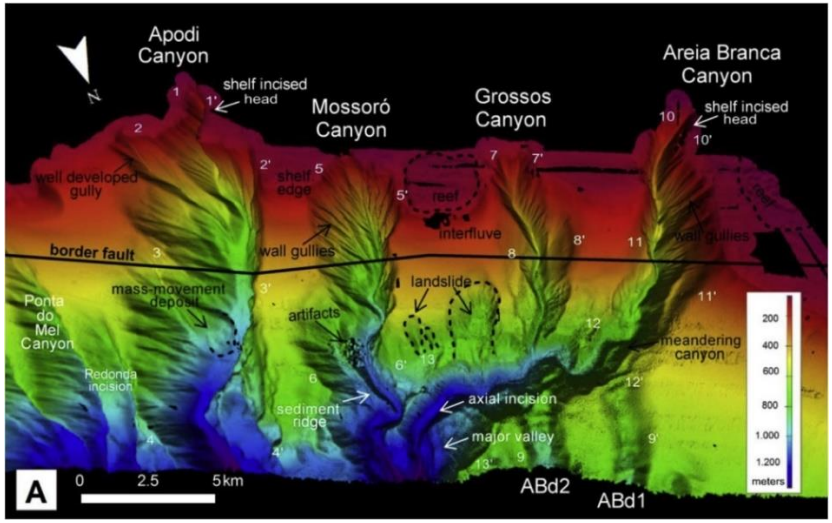
Grossos	2011	50	de Almedia et al. 2015[59]		
Mossoro	2011	50	de Almedia et al. 2015[59]	Landslide scars on canyon walls.	

Apodi	2011	50	de Almedia et al. 2015[59]	Mass movement deposit in the canyon axis.	
Ponta do Mel	2011	50	de Almedia et al. 2015[59]		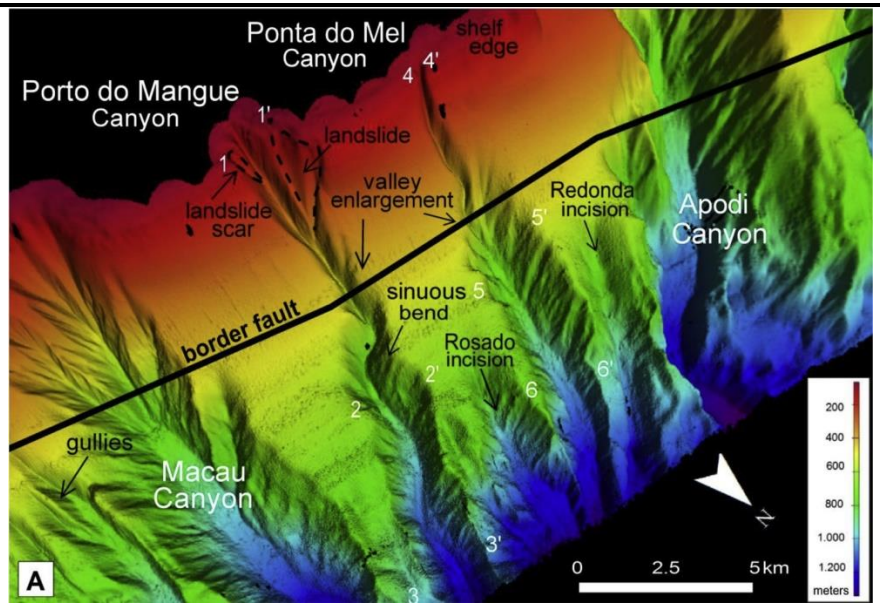
Porto do Mangue	2011	50	de Almedia et al. 2015[59]	Triangular landslide scars in the canyon head	

Macau	2011	50	de Almedia et al. 2015[59]		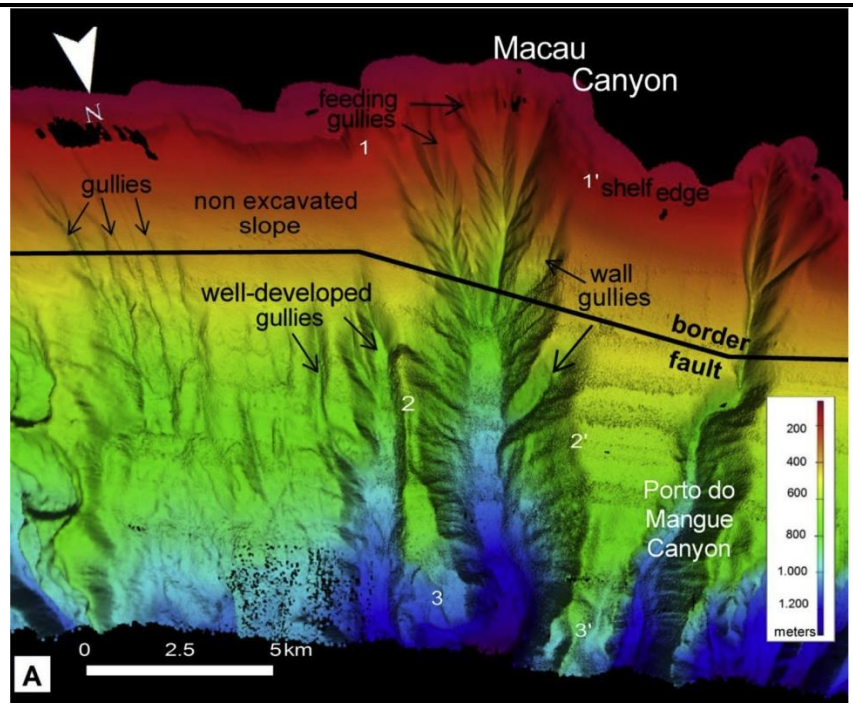

Acu	2011	50	de Almedia et al. 2015[59]	Arcuate headwalls associated with terraces present.	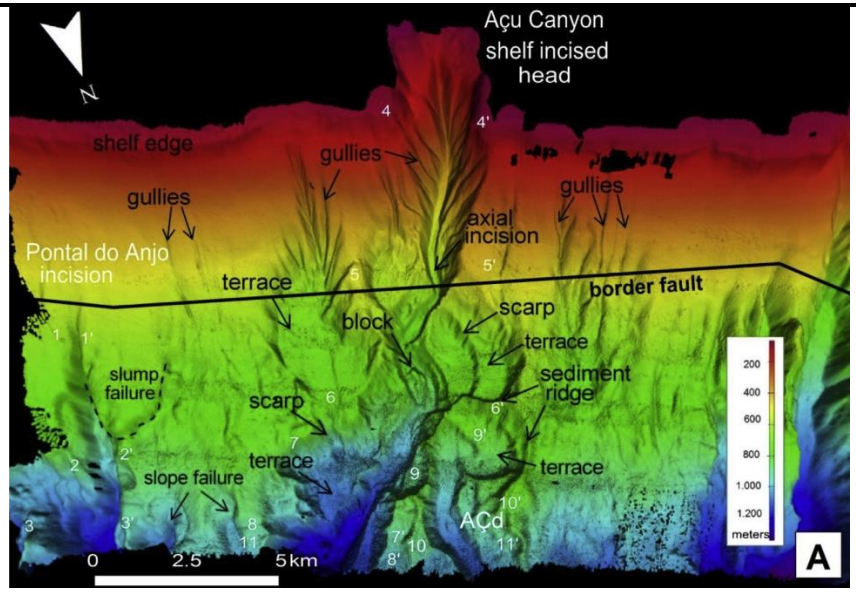

Hattaras Transverse	2005, 2008, 2012	100	Gardner et al. 2016[60]	Landslide scarps and deposits occur across large sections of the canyon. Deposits as high as 25 m down canyon of the confluence of the Hatteras Transverse and Lower Hatteras Canyons have impeded present flow down-canyon.	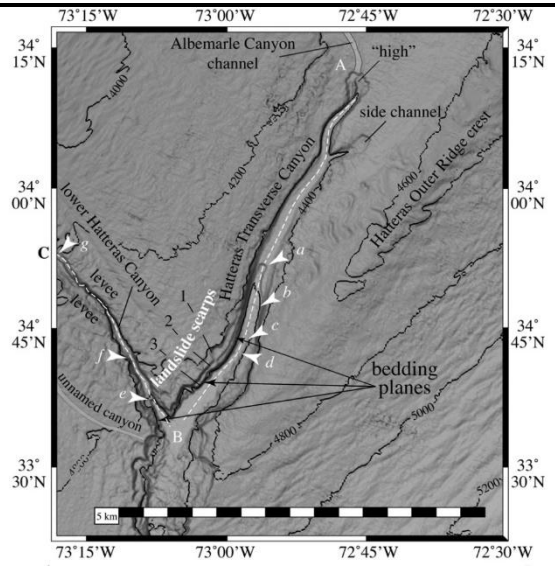 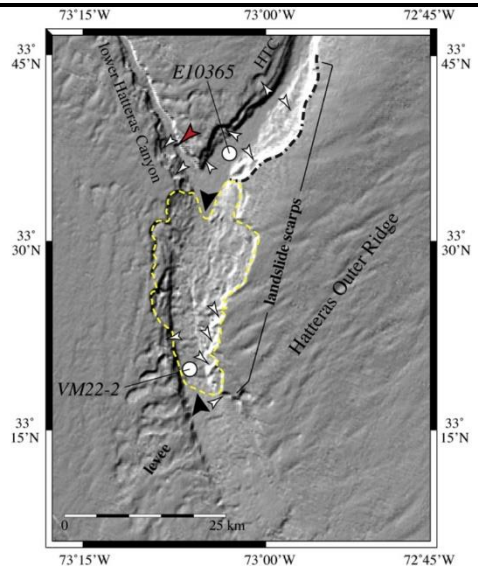
Leven		10	Green and Uken, 2008[61]	Arcuate headwalls in canyon head and on mid-canyon walls.	

			Green, 2011[62]		
Leadsman		10	Green and Uken, 2008[61] Green, 2011[62]	Arcuate headwalls in canyon head and on mid-canyon walls.	
Diepgat		10	Green and Uken, 2008[61] Green, 2011[62]	Arcuate headwalls and terraces identifiable.	
Wright		10	Green and Uken, 2008[61] Green, 2011[62]	Arcuate headwalls in canyon head and on mid-canyon walls.	
White Sands		10	Green and Uken, 2008[61]	Landslide deposit visible in channel thalweg in	

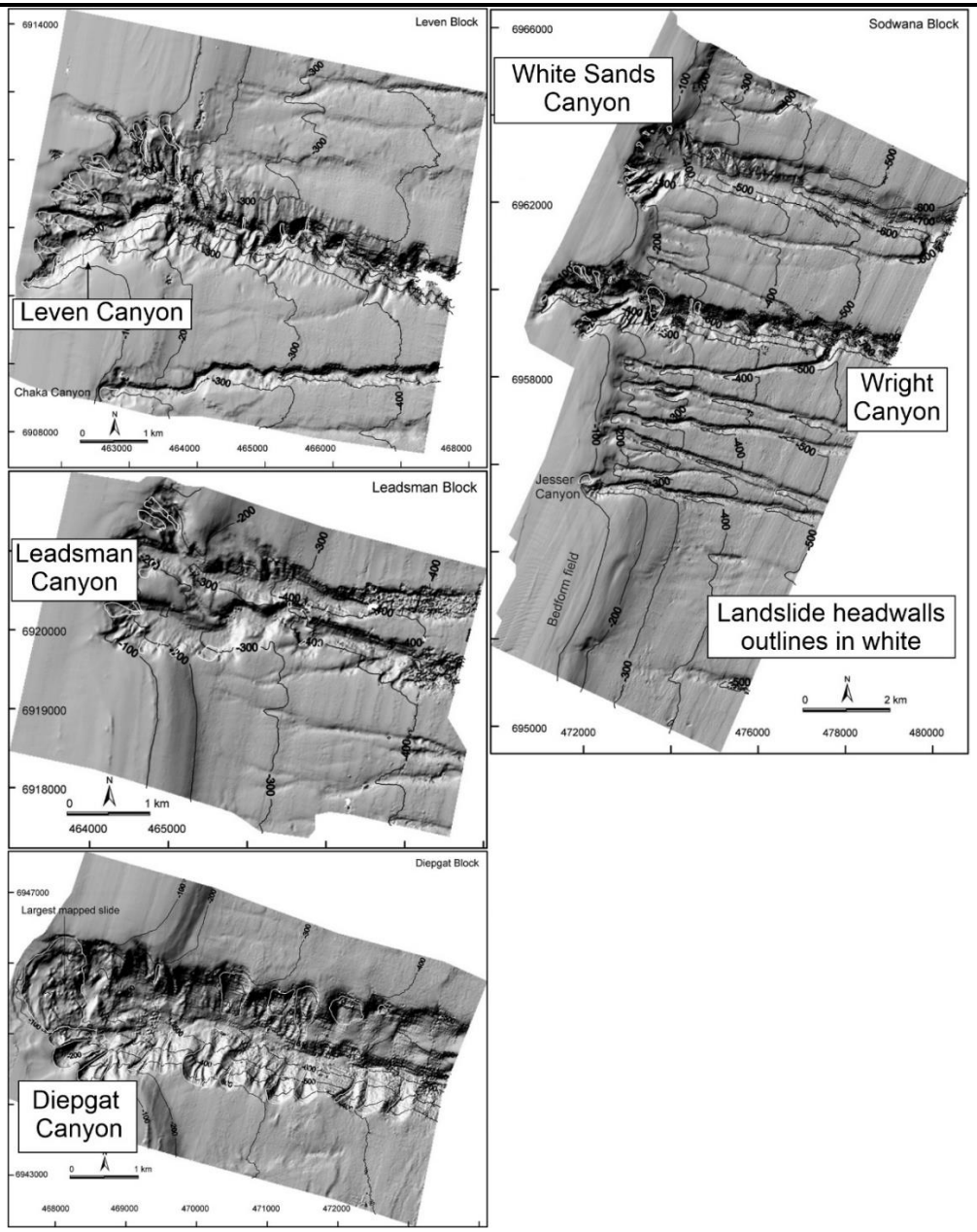

			Green, 2011[62]	seismic reflection data.	
Mabibi		10	Green and Uken, 2008[61] Green, 2011[62]	Arcuate headwalls in canyon and on mid-canyon walls. Slump deposit in the canyon thalweg.	
Sur	1998	25	Harris et al. 2014[63]	Arcuate landslide scars and multiple terraces visible.	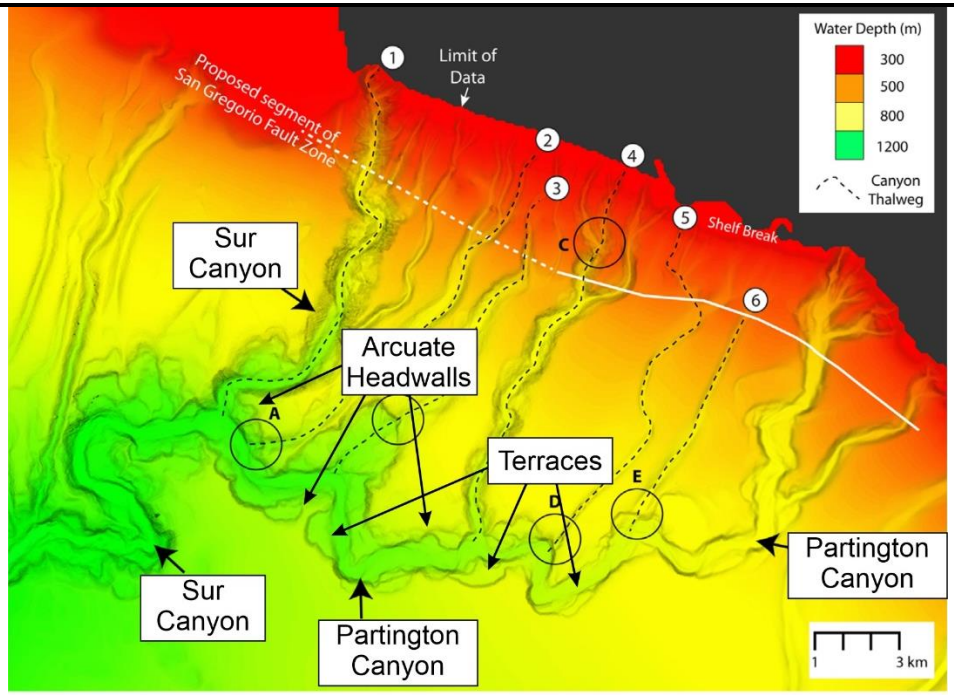
Partington	1998	25	Harris et al. 2014[63]	Arcuate landslide scars and multiple terraces visible.	

Avon	2012		Jimoh et al. 2018[64]	Sidewall scarps and terraces visible.	
Cap de Creus	1995, 2002, 2004	4, 50, 200	Lastras et al. 2007[65]	Side wall slumping leading to narrowing of the canyon thalweg.	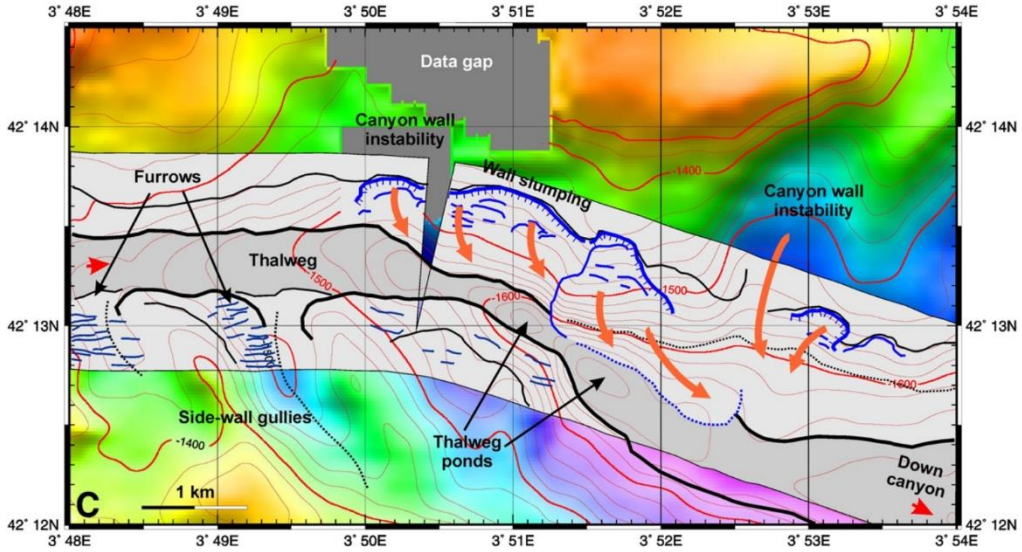
Indus	2008		Clift et al. 2014[66] Li et al. 2018[67]	Terraces and arcuate scars visible. Slump deposits visible in seismic data.	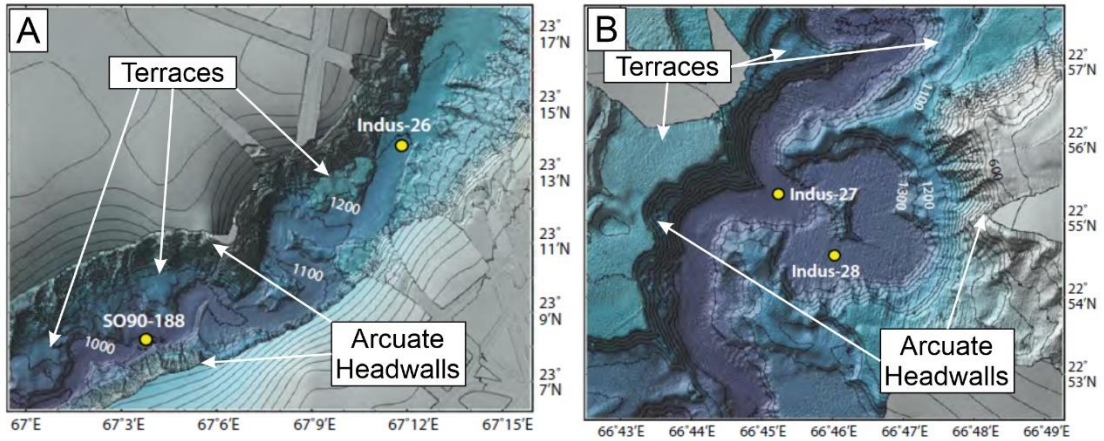

Gaoping			Yeh et al. 2013[68] Liu et al. 2016[69]	Canyon-rim slumping and landslides visible in bathymetry. Slump deposits identified in seismic data.	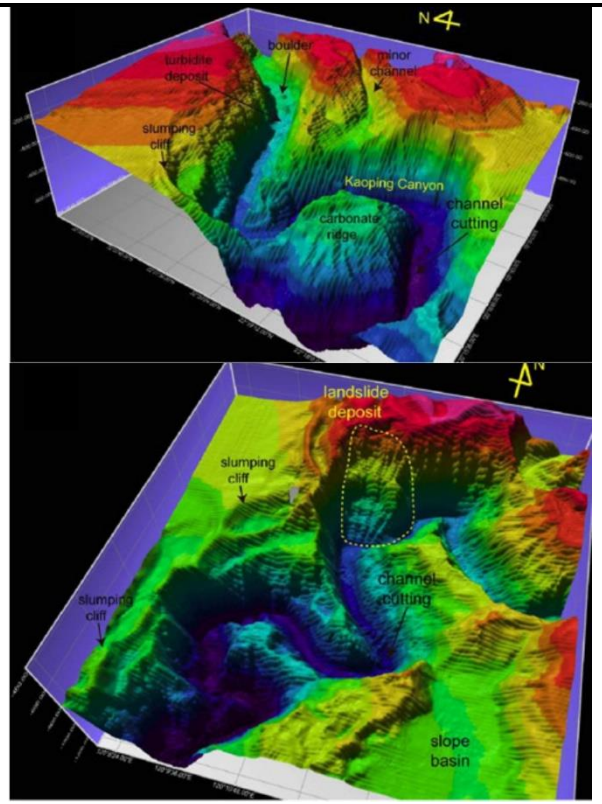	

Mondello	2001, 2004, 2009	15	Lo Iacono et al. 2011[70]	Headscarps present at heads of gullies.	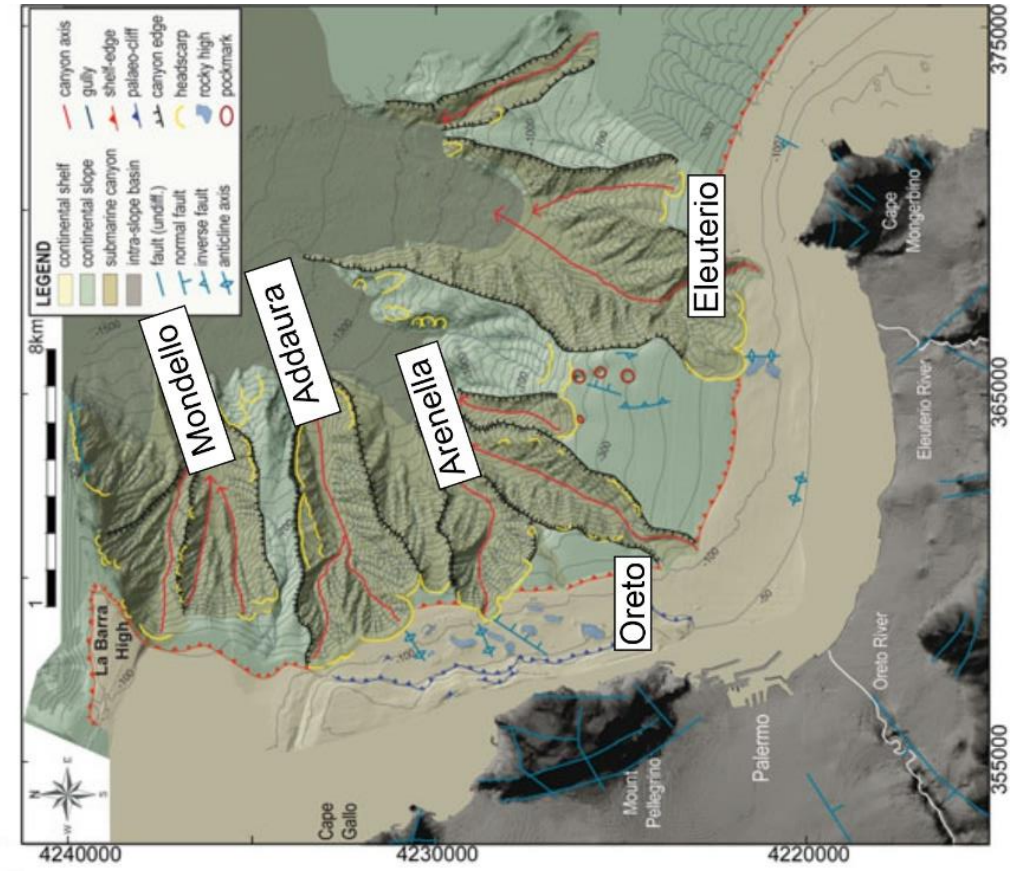
Addaura	2001, 2004, 2009	15	Lo Iacono et al. 2011[70]	Headscarps present along northern wall.	

Oreto	2001, 2004, 2009	15	Lo Iacono et al. 2011[70]	Headscarps visible. Obstruction clearly visible in canyon thalweg.	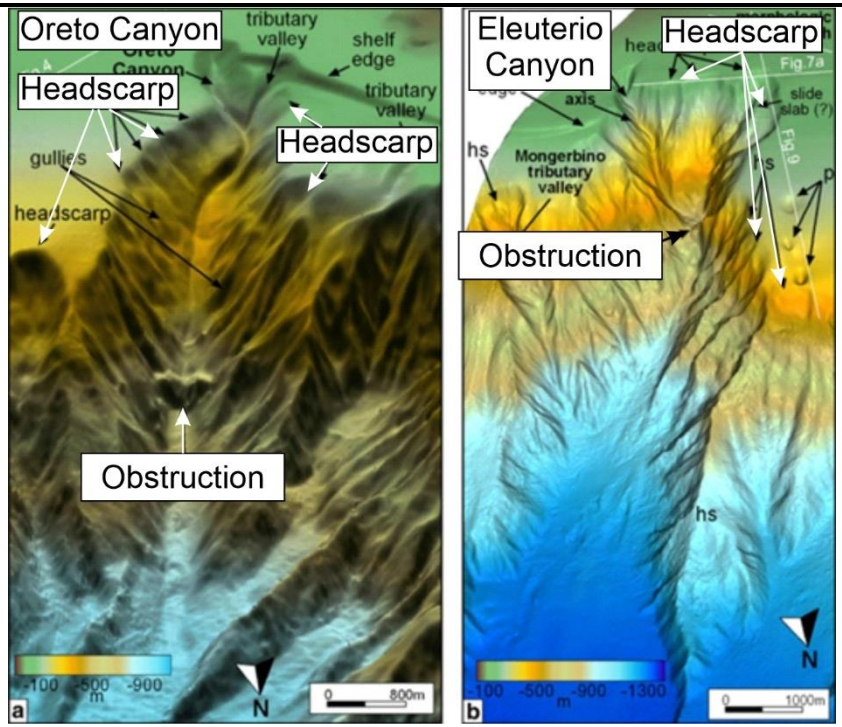
Eleuterio	2001, 2004, 2009	15	Lo Iacono et al. 2011[70]	Headscarps visible. 20 m high obstruction clearly visible in canyon thalweg.	
Cook	2002, 2005	10	Micallef et al. 2013[71]	Landslide scars clearly visible in bathymetry.	
Nicholson	2002, 2005	10	Micallef et al. 2013[71]	Landslide scars clearly visible in bathymetry.	
Wairarapa	2002, 2005	10	Micallef et al. 2013[71]	Landslide scars clearly visible in bathymetry.	

Campbell	2002, 2005	10	Micallef et al. 2013[71]	Landslide scars clearly visible in bathymetry.	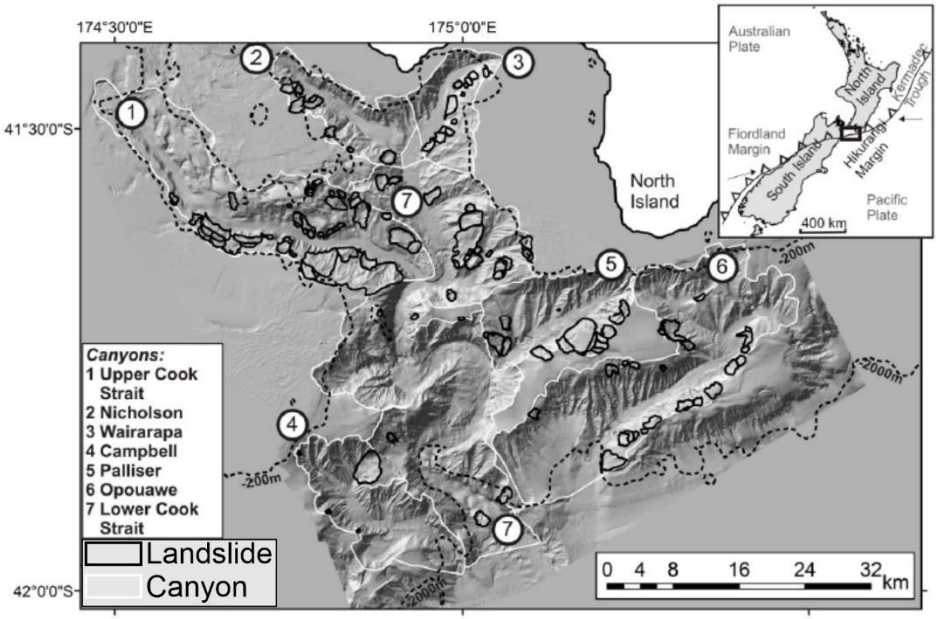
Palliser	2002, 2005	10	Micallef et al. 2013[71]	Landslide scars clearly visible in bathymetry. Landslide blocks are visible on canyon floor.	
Opouawe	2002, 2005	10	Micallef et al. 2013[71]	Landslide scars clearly visible in bathymetry.	
Embro Margin	1995, 1999	50	Micallef et al. 2014[72]	Slide scars visible in bathymetry. Multiple terrace levels visible.	
Mona	1995, 2004	150	Mondziel et al. 2010[73]	Landslide headscarps visible. Slump deposits	

				visible in seismic data.	
Kaikoura	2018 (Repeat bathymetry)	25	Mountjoy et al. 2018[11]	Canyon rim landslide evacuated through the canyon triggered by an earthquake.	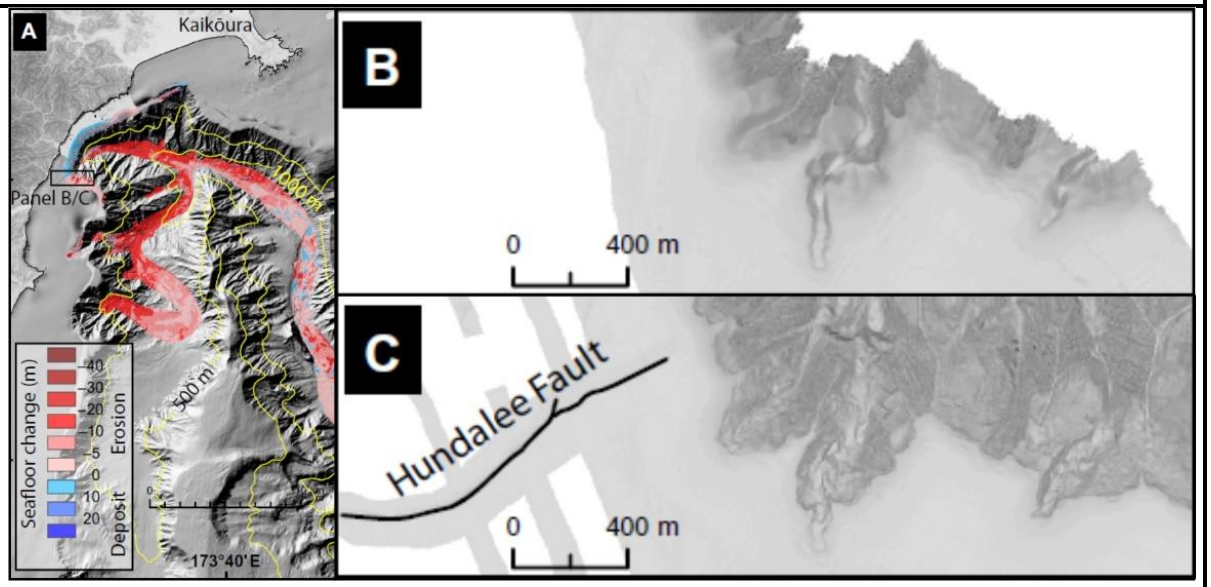

Perth	2014, 2015, 2017, 2018 (Repeat bathymetry in some areas)	20	Nanson et al. 2022[74]	Landslide scars visible. Repeat bathymetry shows failures of some canyon headwalls due to earthquakes. Small accumulations of slump deposits visible in thalweg.	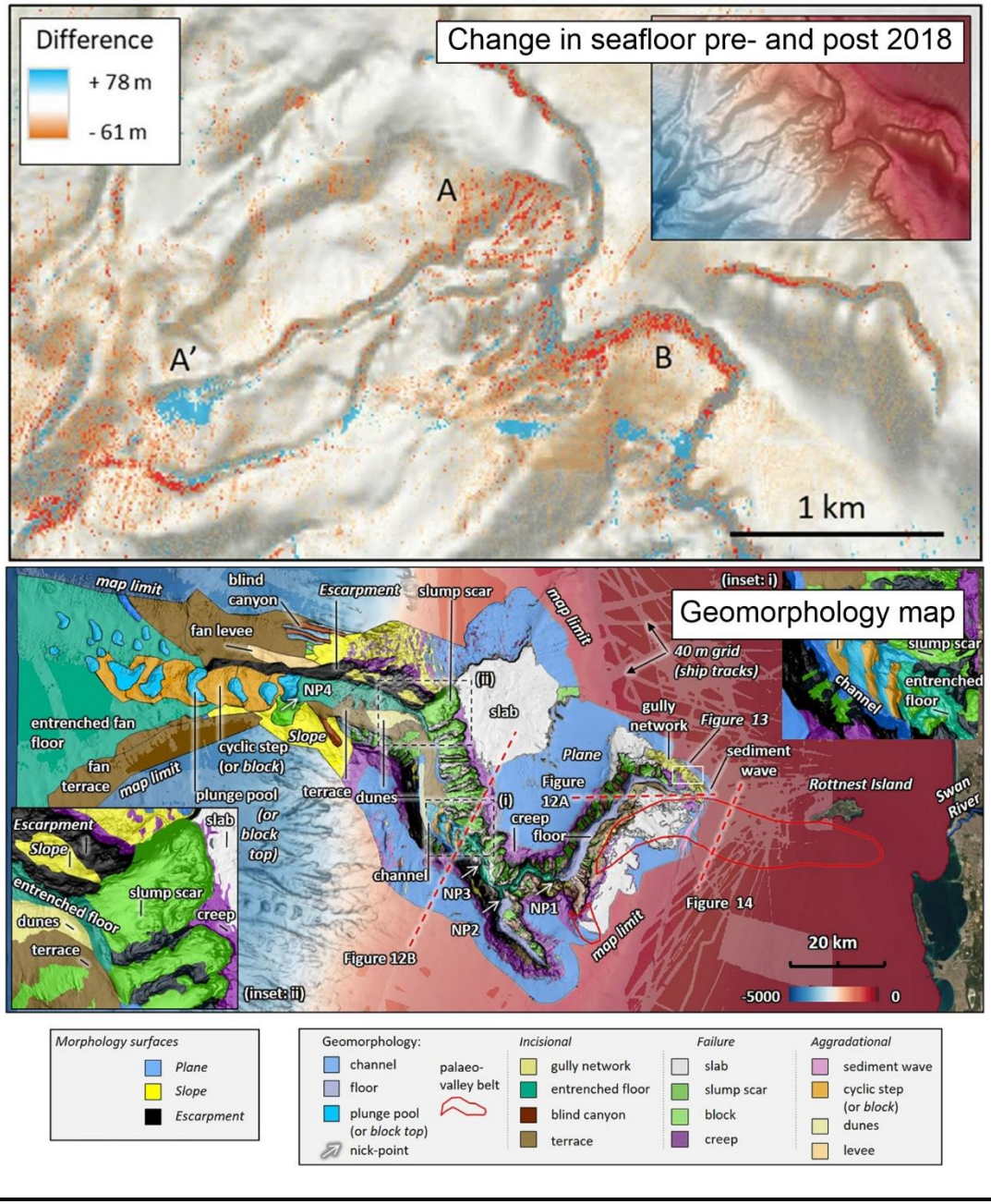

Pont-des-Monts	2007, 2012 (Repeat bathymetry)	3	Normandeau et al. 2014[75]	Small scarps are visible.		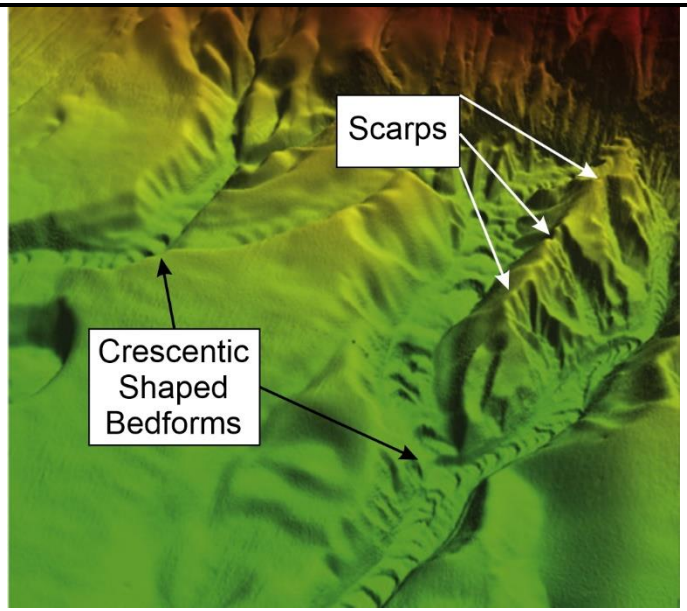

Goto	2008	25	Oiwane et al. 2011[76]	Landslide headwalls observed in bathymetry.	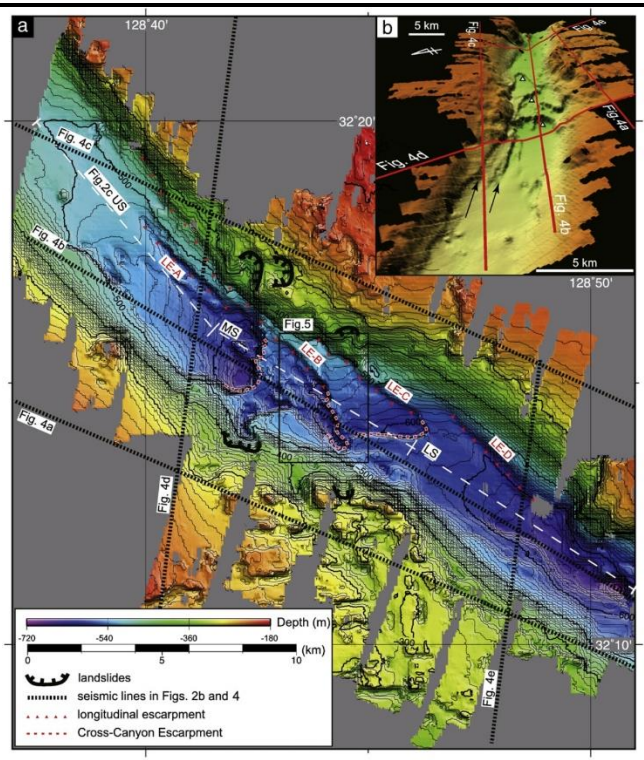

La Jolla	2008	0.7	Paull et al. 2013[77]	Arcuate shaped scarps and terraces clearly visible.	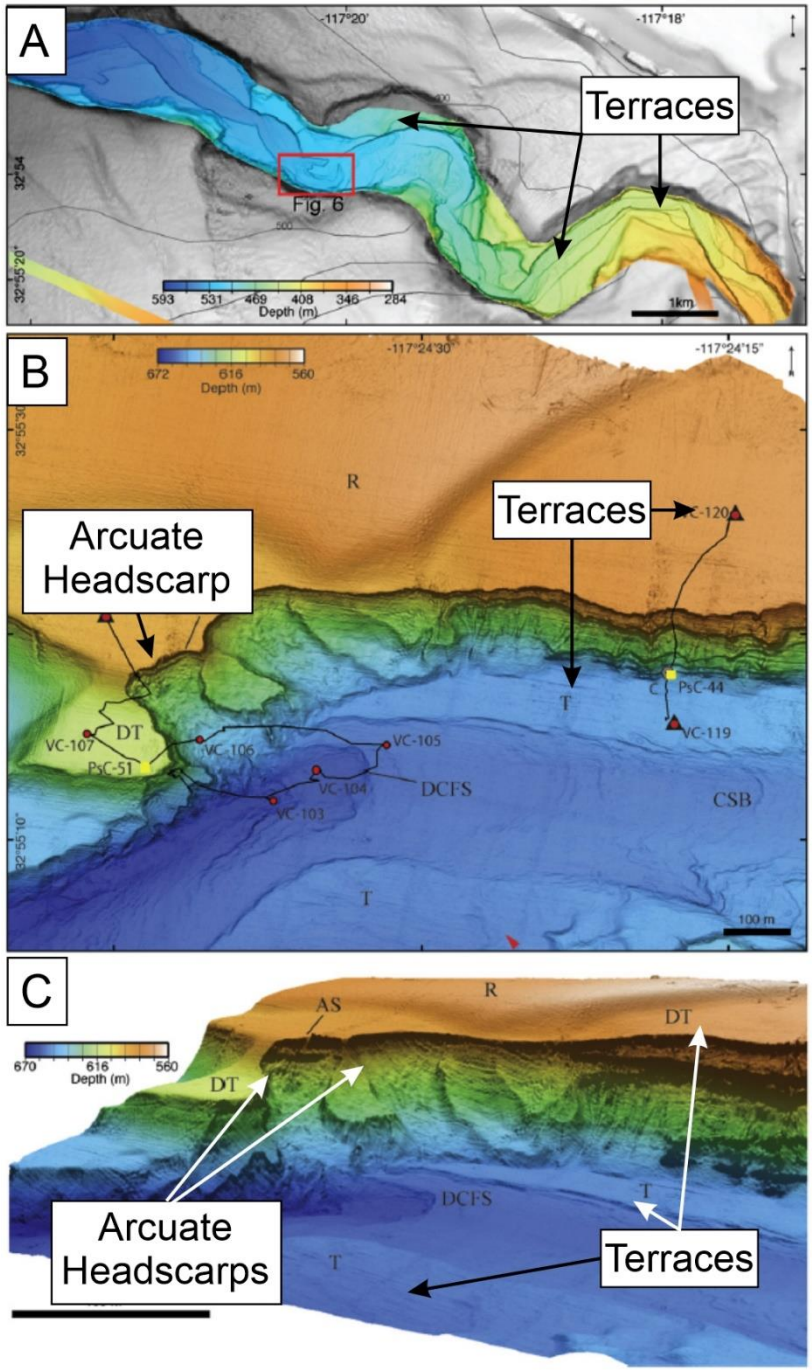

Gioia	2009, 2012	10	Pierdomenico et al. 2016[78]	Landslide headwalls visible.	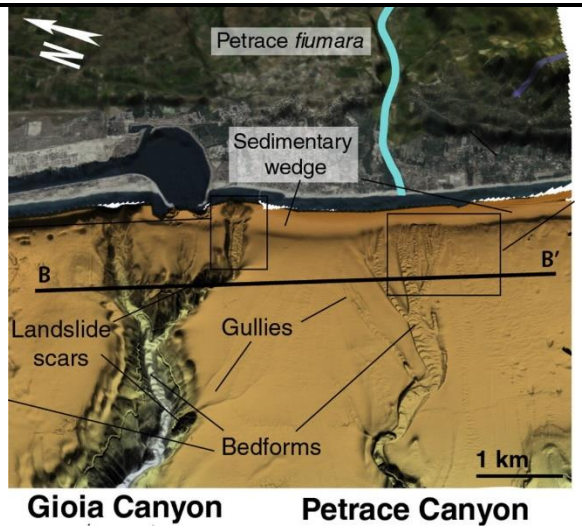

Danube	1998		Popescu et al. 2004[79]	Arcuate scars visible. Evidence of terraces.	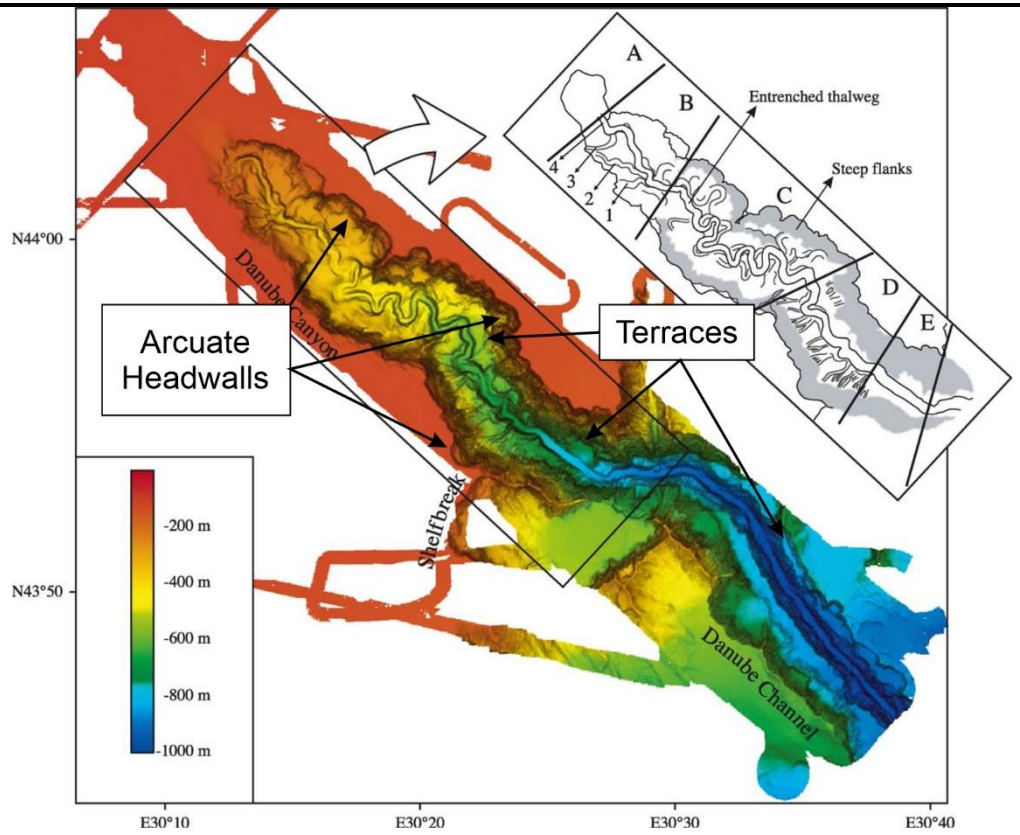

Ribbon Reef	2007	40	Puga Bernabeu et al. 2011[80]	Landslide headwalls visible in bathymetry. Suggested that knickpoints in canyon long profiles may be the result of slide deposits.	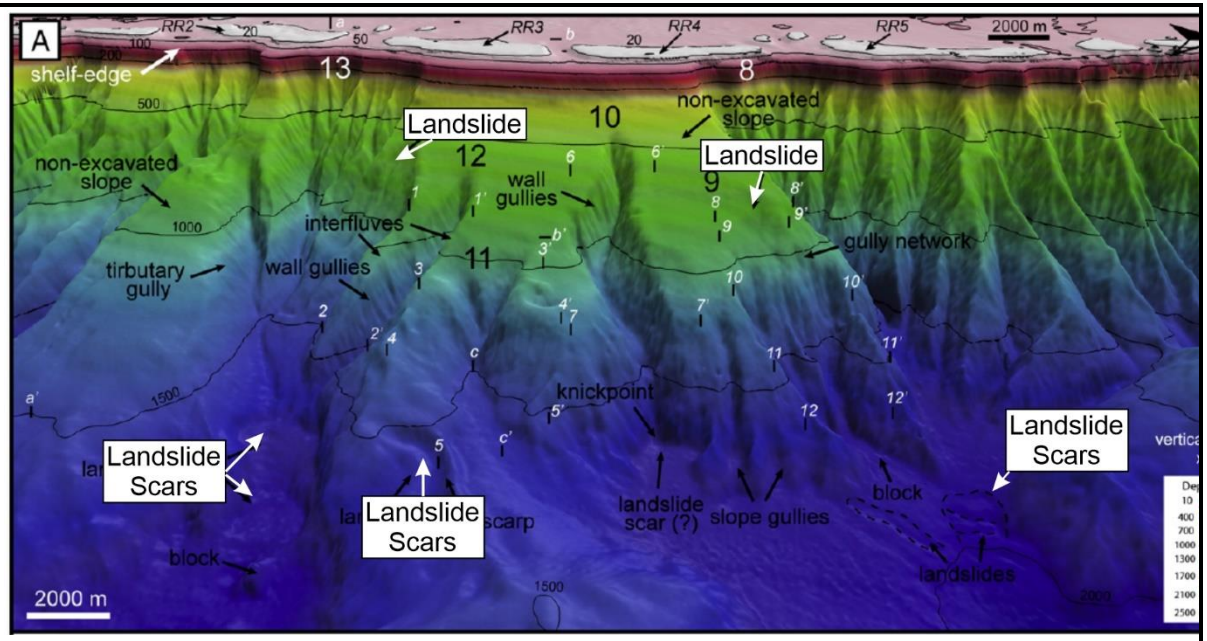
Patia/Mira	2005	60	Ratzov et al. 2012[81]	Headscarps visible in bathymetry. Slump deposit has resulted in a canyon dam and infill visible in seismic data.	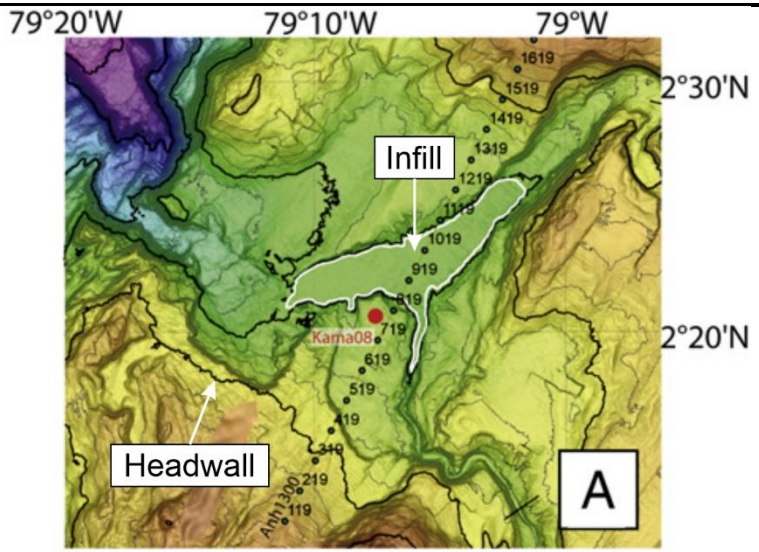

Hudson	2007, 2008, 2009	3	Rona et al. 2015[82]	Landslide scars visible on side walls.	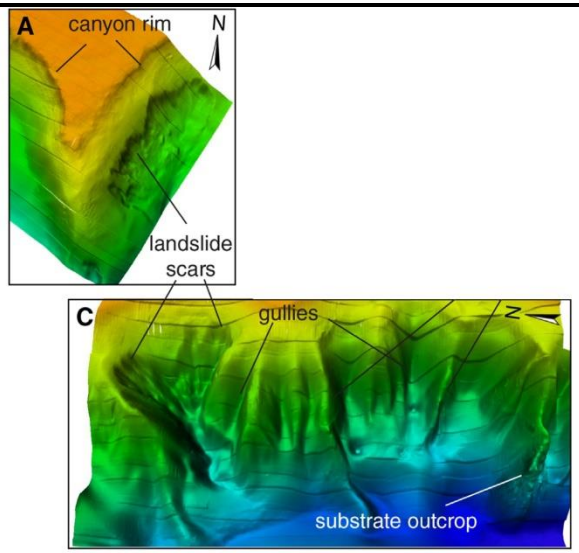
São Vincente	2001 – 2009	250	Serra et al. 2020[83]	Slide scars visible.	
Bahama Bank	2010	20	Tournadour et al. 2017[84]	Arcuate scarps visible.	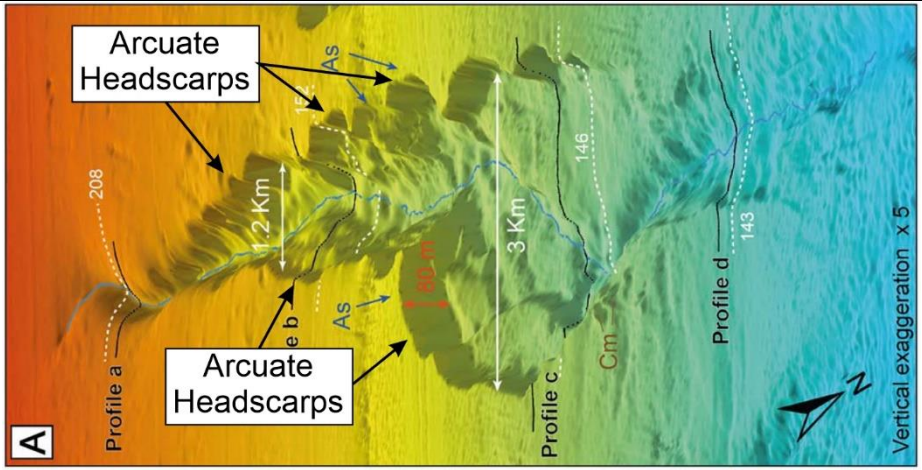

Mozambique Channel	2014	40	Wiles et al. 2019[85]	Mass wasting scars identified on sidewalls.	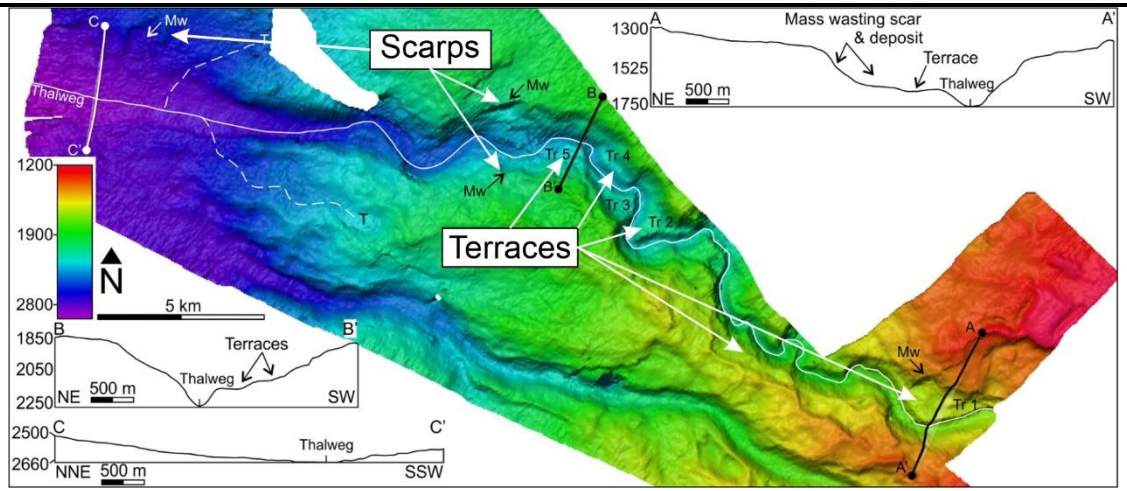
Capbreton	1998, 2020 (Repeat bathymetry)	0.5 - 5	Guiastrennec-Faugas et al. 2020[6]	Arcuate slide scars, slump scars and terraces	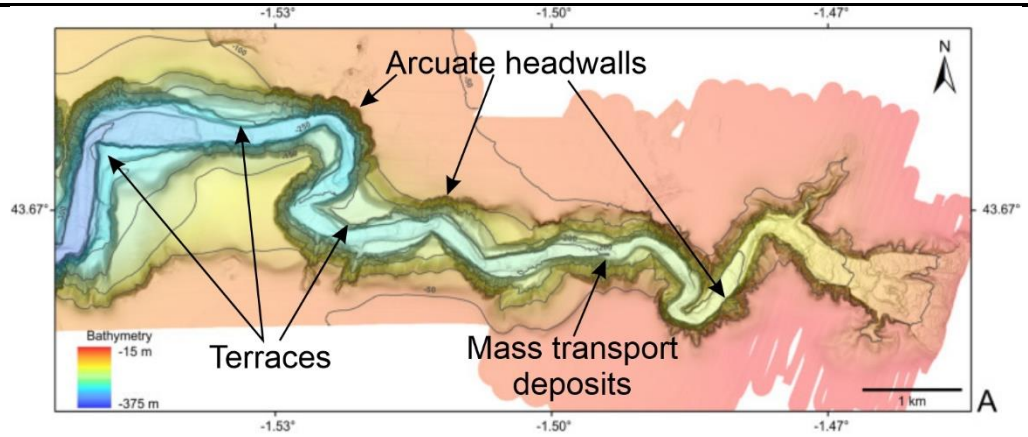
Monterey	2008, 2009	1	Paull et al. 2011[86]	Arcuate scares visible on canyon sidewalls	

Soquel	2008, 2009	1	Paull et al. 2011[86]	Arcuate scares visible on canyon sidewalls	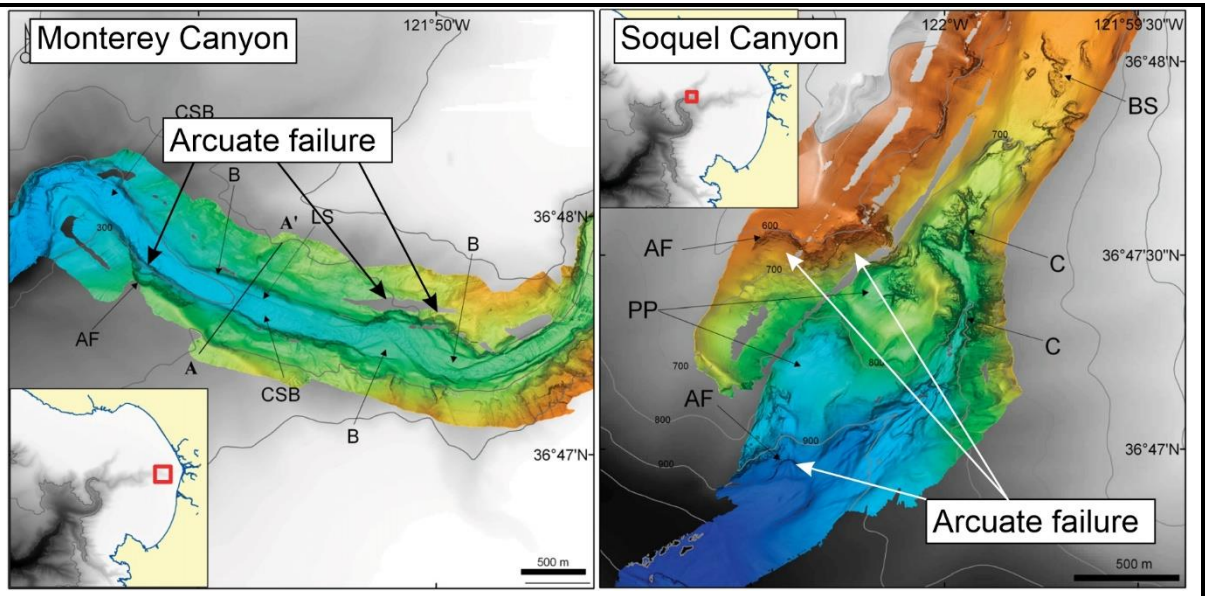

38

39

40

STable. 2. Estimates of sediment and organic carbon masses displaced by submarine mass movement events, flood events and annual discharges from selected large rivers. The table demonstrates the efficiency of sediment and carbon capture and storage by the Congo Canyon landslide-dam.

		Displaced Mass (Mt)	Organic Carbon (Mt C)	Reference
Marine Settings	**Event/Trigger**			
Congo Canyon	Landslide	120±10	3.2 - 3.5 (min 3.1, max 3.8)	This study
Congo Canyon	Infill	170±40	4.6 - 5 (min 3.9, max 6.2)	This study
	Total	290±50	7.8 - 8.5 (min 7, max 10)	This study
Kaikōura Canyon/ Hikurangi Channel	2016 Kaikōura Earthquake/Landslide	850	7	Mountjoy et al. 2018
Continental shelf/ Japan Trench	2011 Tohoku-oki Earthquake/mass movement	360'	>1.73	Kioka et al. 2019
Fluvial Events				
Eel River	1995 flood	25	0.24	Leithold and Hope, 1999
North St. Vrain Creek	2013 flood	0.216	0.01	Rathburn et al. 2017
Kaoping River/Stored on floodplain	2009 Typhoon Morakot flood		0.72*	West et al. 2011
Kaoping River	2009 Typhoon Morakot flood		1.2 - 2.5*	West et al. 2011
Choshui River	2004 Typhoon Mindulle flood	61.4	0.5	Goldsmith et al. 2008
Annual fluvial discharge				
				Baudin et al. 2020
				Coynel et al. 2005
Congo		43	2	Milliman and Farnsworth, 2011
				Bouchez et al. 2014
Amazon		900	11.5	Milliman and Farnsworth, 2011
				Wakeham et al. 2009
				Rosenheim et al. 2013
Mississippi		210	9	Milliman and Farnsworth, 2011
				Li et al. 2015
Yangtze		478	4.4	Milliman and Farnsworth, 2011
				Galy et al. 2008
				Galy and Eglinton, 2011
Ganges/Brahmaputra		1670	8	Milliman and Farnsworth, 2011
				Hilton et al. 2015
Mackenzie		100	2	Milliman and Farnsworth, 2011
				Galy et al. 2015
	Global Total	19,000 ± 500	200 +135/-75	Milliman and Farnsworth, 2011
Notes		*Coarse woody debris		
		'assumes density of 1,300 kg/m3		